Efficient Discovery of Motif Transition Process for Large-Scale Temporal Graphs

Zhiyuan Zheng*
Ocean University of China
Qingdao, China
zhengzhiyuan@stu.ouc.edu.cn

Jianpeng Qi*
Ocean University of China
Qingdao, China
qijianpeng@ouc.edu.cn

Jiantao Li
Ocean University of China
Qingdao, China
ljt7826@stu.ouc.edu.cn

Guoqing Chao
Harbin Institute of Technology
Weihai, China
guoqingchao@hit.edu.cn

Junyu Dong
Ocean University of China
Qingdao, China
dongjunyu@ouc.edu.cn

Yanwei Yu†
Ocean University of China
Qingdao, China
yuyanwei@ouc.edu.cn

Abstract

Understanding the dynamic transition of motifs in temporal graphs is essential for revealing how graph structures evolve over time, identifying critical patterns, and predicting future behaviors, yet existing methods often focus on predefined motifs, limiting their ability to comprehensively capture transitions and interrelationships. We propose a parallel motif transition process discovery algorithm, PTMT, a novel parallel method for discovering motif transition processes in large-scale temporal graphs. PTMT integrates a tree-based framework with the temporal zone partitioning (TZP) strategy, which partitions temporal graphs by time and structure while preserving lossless motif transitions and enabling massive parallelism. PTMT comprises three phases: growth zone parallel expansion, overlap-aware result aggregation, and deterministic encoding of motif transitions, ensuring accurate tracking of dynamic transitions and interactions. Results on 10 real-world datasets demonstrate that PTMT achieves speedups ranging from 12.0× to 50.3× compared to the SOTA method.

Keywords

Large-Scale Temporal Graphs, Motif Transition, Discovery, Parallel

ACM Reference Format:
Zhiyuan Zheng, Jianpeng Qi, Jiantao Li, Guoqing Chao, Junyu Dong, and Yanwei Yu. 2025. Efficient Discovery of Motif Transition Process for Large-Scale Temporal Graphs. In *Proceedings of* . ACM, New York, NY, USA, 14 pages. https://doi.org/XXXXXXX.XXXXXXX

1 Introduction

Motifs are recurring substructures within a graph that typically represent statistical patterns between nodes and edges [13, 42]. The detection and analysis of motifs have broad applications across various fields. For instance, in social networks, motifs help identify interaction patterns among users [42]; in biological networks, motifs assist in uncovering functional relationships between genes or proteins [13]; in cybersecurity, motifs can be used to detect potential anomalous behaviors [12]. These applications highlight the importance of motif detection in understanding the dynamics of complex systems and revealing underlying patterns.

In temporal graphs, where edges and nodes change over time, motifs evolve from static structures to dynamic subgraph patterns, reflecting the shifting nature of relationships within a network [44]. While early studies primarily focused on static graphs [42], recent research underscores the importance of tracking motif evolution to capture temporal dependencies [24]. Understanding how motifs transform over time not only provides critical insights into graph dynamics but also helps in modeling real-world phenomena such as social interactions, disease transmission, and changes in collaborative networks [15, 35]. By examining motif evolution, researchers can identify emerging patterns and predict future structural changes within a graph.

By quantifying motif transition (or evolution) over time, researchers can gain a clearer understanding of how graph structures dynamically change, bridging the gap between static analysis and evolving network behaviors. However, current methodologies for motif transition analysis face several key challenges, particularly when applied to large-scale temporal graphs. *First*, these methods typically suffer from high time complexity. As the graph size and the number of time steps increase, the combinatorial complexity of motif transition increases rapidly, leading to a sharp rise in computational demands and a noticeable drop in algorithm performance [16]. This makes them difficult to use for real-time or near-real-time analysis in large-scale temporal graphs. *Second*, memory consumption is another significant issue, especially when large amounts of temporal data and motif transition trajectories need to be stored, severely limiting the scalability of these methods [33]. *Third*, many existing methods involve redundant computations and inefficient steps, particularly during the dynamic tracking of motif transition, lacking targeted optimizations [34]. This leads to wasted computational resources and prolonged processing times. Thus, a key challenge in quantifying motif transition processes remains.

To address these issues, we propose a parallelized algorithm for discovering motif transition processes. This algorithm leverages

*Zhiyuan Zheng and Jianpeng Qi contribute equally to this work.
†Yanwei Yu is the corresponding author.

,

ACM ISBN 978-1-4503-XXXX-X/2018/06
https://doi.org/XXXXXXX.XXXXXXX

massive parallelism to ensure accurate and efficient identification of motif transitions in large-scale temporal graphs. As part of the parallel framework, it employs a temporal zone partitioning strategy to divide temporal graphs into growth and boundary zones, enabling conflict-free processing and avoiding redundant computations. Additionally, it incorporates overlap-aware result aggregation and deterministic encoding to optimize memory usage and computational efficiency. Results show that our algorithm achieves speedups ranging from 12.0× to 37.3× while maintaining accurate discovery, and it drastically reduces redundant computations. Meanwhile, our method is highly efficient and scalable when processing large-scale temporal graphs. Finally, we also provide a case study to show that capturing motif evolution dynamics is meaningful and provide the results of applying our method. The main contributions of this paper are as follows:

- We present a parallel algorithm for the discovery of motif transitions that guarantees precise counting while substantially enhancing the efficiency of temporal graph analysis. Our method incorporates a temporal zone partitioning strategy, which facilitates the independent identification of motif transition processes across various partitions. This approach maximizes parallelism while maintaining accuracy.
- We address computational bottlenecks in motif transition analysis by reducing redundant computations, lowering time complexity, and minimizing memory overhead. Our method efficiently handles large-scale graphs by leveraging optimized parallel processing and workload distribution.
- We conduct extensive evaluations on large-scale real-world datasets, demonstrating significant performance improvements over existing approaches. Additionally, we provide an in-depth analysis of motif transition dynamics, highlighting how different motifs evolve in temporal graphs and identifying dominant transformation patterns.

2 Related Work

Early seminal work introduced the concept of network motifs as small recurring subgraphs that serve as the fundamental building blocks of complex systems [20, 41, 43]. Subsequent studies further refined static motif analysis by proposing efficient counting techniques based on combinatorial principles [18, 19, 30], as well as algorithms such as ESCAPE [46] and pivoting strategies for 4-node motifs [27]—approaches that have been extended and improved in later works [22, 25, 40]. In parallel, advances in statistical modeling of networks, including mixed membership models [11, 23] and dynamic stochastic blockmodels [54, 55], have provided a probabilistic framework that complements motif-based analyses [14].

With the advent of temporal networks, the focus has shifted toward capturing time-dependent interactions. Formal definitions of δ-temporal motifs were introduced to ensure that the events comprising a motif occur within a specified time window [26, 45], while studies by Kovanen et al. [31, 32] demonstrated that temporal motifs can reveal homophily, gender-specific patterns, and group communication dynamics [29, 51]. Additional investigations have extended these ideas to various domains, including financial networks [37], mobile communication networks [36], and patent collaboration networks [38], thereby underscoring the broad applicability of temporal motif analysis [52, 59].

In parallel to counting, a series of works have explored motif evolution and its application in graph generation. Liu et al. [39] proposed the Motif Transition Model (MTM) that leverages transition probabilities for synthetic temporal graph generation, although its counting module suffers from high computational complexity (e.g., $O(|\mathcal{E}|^3)$ for triangle motifs) [46]. Zhou et al. [60] introduced the TagGen model, which discretizes continuous time into snapshots to capture motif transitions, while other approaches have combined mixed membership models [11, 23] with motif statistics for dynamic network tomography [53]. Additional work on independent temporal motifs for summarizing networks [48, 49] and analytical models for motif transitions [47, 50] has further advanced the field.

Moreover, to accelerate the counting process, Gao et al. [21] developed a framework that exploits sparse matrix operations for batch counting of heterogeneous motifs, and recent advances in parallel and GPU-accelerated computing [57, 58] have contributed to efficient processing of large-scale temporal graphs. Complementary contributions by Jin et al. [28], Viswanath et al. [52], and Zeno et al. [56] have examined motif dynamics in social and communication networks, thereby offering insights that span a variety of real-world applications [17].

However, challenges remain in fully capturing the continuous evolution of motifs and in developing scalable methods for their efficient enumeration. Therefore, our work aims to bridge this gap by proposing a parallelized motif transition process path discovery algorithm that directly models dynamic transitions and substantially reduces computational overhead.

3 Preliminary and Problem Definition

In this section, we first introduce some preliminaries, including the definitions of *temporal graph*, *δ-temporal motif*, *motif transition*, and *motif transition process*. Then, we present the problem that needs to be solved, *i.e.*, *motif transition process discovery*.

Definition 1 (Temporal Graph [21]). *A temporal graph is a dynamic network represented as $\mathcal{G} = (\mathcal{V}, \mathcal{E}, \mathcal{T})$, where $\mathcal{V}$, $\mathcal{E}$, and $\mathcal{T}$ denote the node set, the temporal edge set and the timestamp collection, respectively. Each directed temporal edge $e^t_{ij} = (v_i, v_j, t)$ records an interaction from node v_i to v_j at timestamp $t \in \mathcal{T}$.*

Definition 2 (δ-temporal Motif). *A δ-temporal motif is defined as a temporally ordered sequence of l edges that form a connected subgraph comprising k nodes. Formally, such a δ-temporal motif is represented as $M = \langle (u_1, v_1, t_1), (u_2, v_2, t_2), \ldots, (u_l, v_l, t_l) \rangle, t_1 \leq t_2 \cdots \leq t_l$, where $t_i - t_{i-1} \leq \delta$ for every i such that $2 \leq i \leq l$.*

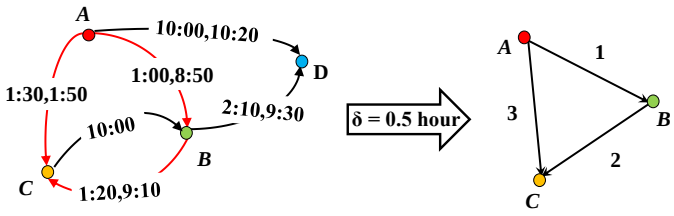

Figure 1: An example of a δ-temporal motif ($\delta = 0.5$ hours).

Example: Consider the interactions among nodes A, B, and C as depicted in Figure 1. Given $\delta = 0.5$ hours, the following temporally

ordered sequence of edges $M = \langle (A, B, 1{:}00), (B, C, 1{:}20), (A, C, 1{:}30) \rangle$ is valid 3-node δ-temporal motif because the time interval between any two adjacent edges is less than the given $\delta = 0.5$ hours, and the static projection of this sequence forms a connected subgraph – a triangle.

Definition 3 (Motif Transition). *A motif transition $T(M \to M')$ is defined as the process by which a δ-temporal motif M with l edges evolves into another δ-temporal motif M' with $l+1$ edges via the addition of a new temporal edge $e_{new} = (u, v, t_{l+1})$, subject to the following conditions:*

- *$t_{l+1} > t_l$, where t_l is the timestamp of the last edge in M.*
- *$\{u, v\} \cap \mathcal{V}(M) \neq \emptyset$, indicating that at least one endpoint of e_{new} belongs to the vertex set of M, i.e., $\mathcal{V}(M)$.*
- *There does not exist any earlier valid transition $T(M \to M'')$ prior to time t_{l+1}.*

Definition 4 (Motif Transition Process [39]). *In a given temporal graph $\mathcal{G}$, a motif transition process is defined as a sequence of motif transitions, $T(M^1 \to \cdots \to M_i^l \to S)$, w.r.t. a transition size limit $l_{\max}$ and a transition time limit δ, where S denotes the stopping state. The process starts with a 1-edge temporal motif and ends at M_i^l if either of the following conditions holds:*

- *The motif M_i^l reaches the maximum allowed number of edges, i.e., $l = l_{\max}$.*
- *Within the time window $(t_l, t_l + \delta]$, where t_l is the timestamp of the last edge in M_i^l, no new edge e_{l+1} is available to create the next motif transition $T(M_i^l \to M_j^{l+1})$.*

Example: Figure 2 illustrates an edge-to-triangle motif transition process derived from Figure 1. In this example, the initial δ-temporal motif $M_1 = \langle A \to C \rangle$ evolves into $M_2 = \langle A \to B, B \to C \rangle$ and subsequently into $M_3 = \langle A \to B, B \to C, A \to C \rangle$, under the constraints of $\delta = 0.5$ hours and $l_{\max} = 3$. This motif transition pattern frequently appears in social network interactions where triadic closure strengthens community bonds.

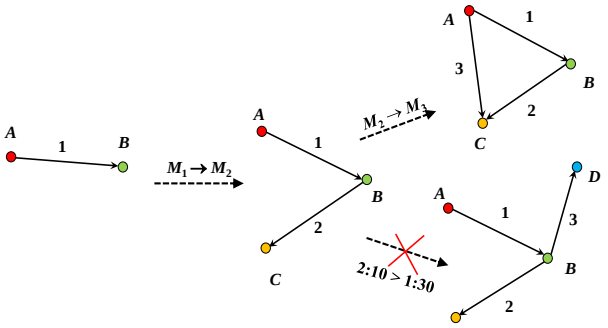

Figure 2: A example of motif transition process ends as a triangle temporal motif (δ = 0.5 hours, $l_{\max}$ = 3).

The motif transition time $\Delta t = t_{l+1} - t_l$ quantifies the waiting period between motif evolutions. Motif transition process can reveal network dynamics, for instance, rapid triangle closures may indicate coordinated behavior in financial networks.

Problem (Motif Transition Process Discovery). *Given a temporal graph $\mathcal{G}$, temporal constraint δ, and transition size limit $l_{\max}$, motif transition process discovery is to exactly record all motif transition processes in $\mathcal{G}$.*

By aggregating the transition counts of all specified temporal motifs, we can obtain a complete statistical profile of the entire motif transition processes. This formalism provides the foundation for analyzing temporal network evolution patterns at scale.

4 Methodology

Our motif-transition process (MTP) discovery framework begins with a temporal graph $\mathcal{G}$, which is then partitioned into independent zones using our zone partition strategy (Section 4.1). Then, in Section 4.2, we adopt a parallel algorithm to assign them to different threads. Within each zone, we extract all MTPs that satisfy the constraints. After multi-threading, in the global merge step, we use the "first-zone" principle for conflict resolution, ensuring that each motif transition is uniquely and accurately counted. Finally, the complete set of motif transitions is discovered and reported. The workflow is shown in Figure3.

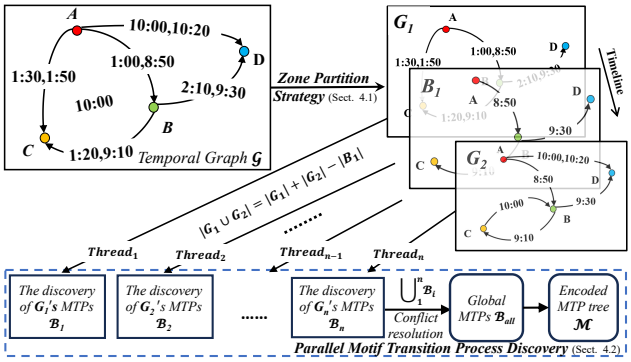

Figure 3: Motif-transition process discovery workflow.

4.1 Zone Partition Strategy

On large-scale temporal graph, we adopt the data parallelism, i.e., partition the graph, approach to accelerate the discovery process. However, data parallelism requires an effective temporal partitioning scheme that avoids over-counting motifs at partition boundaries. We propose the Temporal Zone Partitioning (TZP) strategy, which divides the temporal graph into interleaved *Growth Zones* and *Boundary Zones*. Growth Zones support independent parallel processing, while Boundary Zones capture cross-partition motifs and, by applying a "first-zone" rule, ensure that each motif transition is uniquely assigned to one Growth Zone. This design both enforces strict computational boundaries and eliminates duplicate counts.

Definition 5 (Growth Zone). *Given parameters ω (temporal expansion factor), δ (maximum motif duration), and $l_{\max}$ (transition size limit), a growth zone G_i is defined as a temporal segment spanning $L_g = \omega \cdot \delta \cdot l_{\max}$ time units.*

Definition 6 (Boundary Zone). *The boundary zone B_i between consecutive growth zones G_i and G_{i+1} is an overlapping temporal buffer of length $L_b = \delta \cdot l_{\max}$. It spans:*

$$[t_{end}(G_i) - L_b, t_{end}(G_i)] \tag{1}$$

The TZP strategy operates as a linear scan through the temporal edges, creating interleaved growth and boundary zones. As illustrated in Figure 4, this process partitions the graph such that the growth zones (green) can be processed independently, while the boundary zones (orange) capture motif transition processes that span across partitions. The choice of ω balances zone independence and computational granularity—larger values reduce inter-zone communication but increase memory usage per partition. Through empirical analysis, we found that $\omega = 20$ offers an optimal trade-off for most real-world networks.

Algorithm 1 Temporal Zone Partitioning (TZP) Strategy

Require: Temporal edge set $\mathcal{E}$, δ, $l_{\max}$, ω
Ensure: Partition set $\mathcal{Q} = \{G_1, B_1, G_2, B_2, ...\}$
1: Initialize $t_{\text{start}} \leftarrow \min\{e.time | e \in \mathcal{E}\}$
2: **while** $t_{\text{start}} \leq \max\{e.time | e \in \mathcal{E}\}$ **do**
3: Compute zone boundary: $t_{\text{end}} \leftarrow t_{\text{start}} + L_g$
4: Extract growth zone: $G_i \leftarrow \{e \in \mathcal{E} | t_{\text{start}} \leq e.time < t_{\text{end}}\}$
5: Construct boundary zone by Eq.(1)
6: Append to partition set: $\mathcal{Q}$.add(G_i, B_i)
7: $t_{\text{start}} \leftarrow t_{\text{end}}$
8: **end while**
9: **return** $\mathcal{Q}$

Lemma 4.1 (Uniqueness of motif transition attribution). *1] For any δ-temporal motif instance $M = \langle e_1, \ldots, e_l \rangle$ produced by Algorithm 1, the motif transition is confined entirely within a single growth zone G_i.*

Proof. By the δ-temporal motif definition (Def. 2), the total time span of M satisfies $\Delta t = t_l - t_1 \leq l * \delta$. We consider two cases:

(1) **Case 1:** If all edges of M reside within a single growth zone G_i, then clearly $M \subseteq G_i$.
(2) **Case 2:** If M spans multiple zones, let e_j be the first edge that crosses into the adjacent growth zone G_{i+1}. By design, the mechanism captures such edges within the boundary zone B_i, which is the overlapping region between G_i and G_{i+1}. Consequently, even if M extends into G_{i+1}, the overlapping segment B_i is attributed to G_i according to the "first-zone" principle. Hence, M is uniquely associated with G_i.

□

Lemma 4.2 (Completeness of motif transition processes). *For any instance of motif transition process $T = \langle M^1 \rightarrow M^2 \rightarrow \ldots \rightarrow M^l \rangle$, it guarantees that T is entirely captured by one of the following three cases, and that the overall counting can be computed exactly using the inclusion-exclusion principle:*

$$|G_i \cup G_{i+1}| = |G_i| + |G_{i+1}| - |B_i|,$$

where G_i and G_{i+1} denote the counts from adjacent growth zones, and B_i is the count from their shared boundary zone.

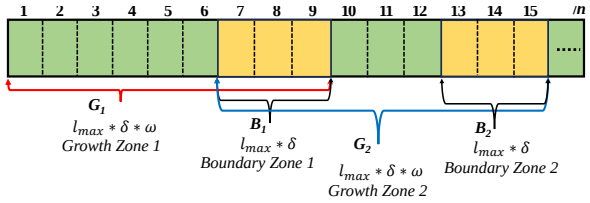

Figure 4: An example of TZP strategy ($\omega = 3$, $\delta = 1$hr, $l_{\max} = 3$). Growth zones (green) enable independent processing, while boundary zones (orange) capture cross-partition motifs.

Proof. Let $\Delta t = t_l - t_1 \leq l * \delta$ by the definition of a δ-temporal motif transition.By Lemma 4.1 We consider three mutually exclusive cases:

- Case 1: **Motif transition entirely within a single growth zone.** If all edges of T reside within a single growth zone G_i, then trivially, $T \subseteq G_i$ and is counted exactly once.
- *Case 2:* **Motif transition extending from a growth zone into its boundary zone.** If T begins in a growth zone G_i and extends into the corresponding boundary zone B_i, then the algorithm ensures that the motif transition is fully captured within $G_i \cup B_i$. In this case, the motif transition is counted only once, as the extension into B_i does not lead to additional, separate counts.
- Case 3: **Motif transition spanning from a boundary zone into the next growth zone.** If T spans from the boundary zone B_i into the subsequent growth zone G_{i+1}, then T is naturally counted in both B_i and G_{i+1}. To correct for this double counting, we apply the inclusion-exclusion principle by subtracting the overlapping count in B_i. That is, the unique count for these transitions is given by

$$\text{Count} = |G_i| + |G_{i+1}| - |B_i|.$$

Thus, by considering these three cases and applying the inclusion-exclusion principle, the partitioning mechanism ensures that every δ-temporal motif transition is uniquely and completely counted without any omissions or duplications. □

As shown in Figure 5, the given temporal graph is partitioned into corresponding subgraphs based on its growth zones and boundary zones. After independently mining for motif transitions in each subgraph, the combined result—obtained by adding the statistics from the G_1 subgraph to those from the G_2 subgraph and then subtracting the statistics from the B_1 subgraph—exactly equals the overall motif transition statistics of the original temporal graph. A detailed analysis of the motif count reconciliation process can be found in Appendix B.

4.2 Parallel Motif Transition Process Discovery

In Section 4.1, we divide the temporal graph into subgraphs (i.e., partitions) that can be counted independently and accurately. In this section, we introduce our parallel motif transition process discovery algorithm, namely PTMT. PTMT employs *three phases* to overcome the limited parallelism and scaling challenges of previous approaches. It enables parallel counting of motif transitions across all subgraphs.

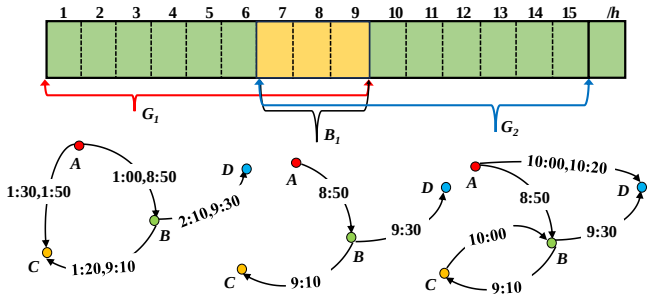

Figure 5: Visualization of temporal graph partitioning

4.2.1 Three-Phase of Parallel Motif Transition Process Discovery. **Phase 1: Growth Zone Parallel Expansion.** Each thread processes its assigned growth zone by iterating over its temporal edges in chronological order. For each edge e, we use a function `try_to_transit()`, which takes e, δ, $l_{\max}$, and the current candidate motif transition set $\mathcal{B}_k$ as inputs, to extract the next transition if there exists. Specifically, it examines whether appending e to any existing transition in $\mathcal{B}_k$ satisfies the two key constraints: The temporal constraint, which requires that the time difference between e and the last edge of the transition is at most δ, and the size constraint, which ensures that the extended transition does not exceed $l_{\max}$ transitions (or edges). If both conditions are met, the function returns the new candidate transitions generated by appending e, and these are then merged into $\mathcal{B}_k$ via the update $\mathcal{B}_k \leftarrow \mathcal{B}_k \cup \texttt{try\_to\_transit}(e, \delta, l_{\max}, \mathcal{B}_k)$.

Phase 2: Overlap-Aware Result Aggregation. Due to overlapping regions (i.e., boundary zones B_i), candidate motifs may be duplicated. These duplicates are eliminated by performing local deduplication in the boundary zones followed by an atomic global merge. This mechanism enforces the "first-zone" principle, ensuring each motif is counted only once.

Phase 3: Deterministic Relabeling Encoding. Candidate motifs are encoded into fixed-length strings using a deterministic relabeling scheme that maps original node IDs to contiguous identifiers and concatenates them in temporal order. Specifically, for a candidate motif represented as $\langle (u_1, v_1, t_1), (u_2, v_2, t_2), \ldots, (u_n, v_n, t_n) \rangle$, the encoding is defined as $\bigoplus_{i=1}^{n} (f(u_i) \oplus f(v_i))$, where $f : \mathcal{V} \to \mathbb{N}$ assigns a unique numerical string to each vertex upon its first occurrence and $\oplus$ denotes string concatenation. This compact encoding enables efficient $O(1)$ hash table lookups for frequency counting, thereby eliminating the need for costly graph isomorphism checks.

After the three phases, it produces the final output, as illustrated in the example below. Figure 6 visualizes a motif transition tree rooted at the 2-edge motif "0101". Each branch corresponds to a distinct transition path under the constraints. Specifically:

- **Triangle Formation:** The transition path 0101 → 010110 accounts for 62% of the transitions.
- **Chain Extension:** The transition path 0101 → 010102 accounts for 28% of the transitions.
- **Reciprocal Edge:** The transition path 0101 → 010101 accounts for 10% of the transitions.

This string-coded representation provides an intuitive visualization of the motif transition process and facilitates further analysis and interpretation of the transition dynamics.

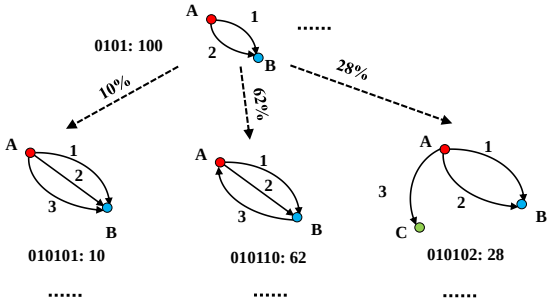

Figure 6: Motif transition tree with string-coded types

Algorithm 2 Parallel Tree Motif Transition Discovery (PTMT)

Require: Temporal edges $\mathcal{E}$, time threshold δ, transition size limit $l_{\max}$, window parameter ω, number of threads #threads
Ensure: Motifs quantities map $\mathcal{M}$
1: Partition edges into zones: $\mathcal{Q} \leftarrow$ Algorithm 1$(\mathcal{E}, \delta, l_{\max}, \omega)$
2: **OpenMP Parallel For** each zone $Z_k \in \mathcal{Q}$: ▷ **Phase 1**
3: Initialize an empty candidate set $\mathcal{B}_k$
4: **for** each edge $e \in Z_k$ in temporal order **do**
5: $\quad \mathcal{B}_k \leftarrow \mathcal{B}_k \cup$ try_to_transit$(e, \delta, l_{\max}, \mathcal{B}_k)$
6: **end for**
7: Global merge: $\mathcal{B}_{\text{all}} \leftarrow \bigcup_k \mathcal{B}_k$ with conflict resolution ▷ **Phase 2**
8: Encode motifs: $\mathcal{M} \leftarrow$ DigitEncode$(\mathcal{B}_{\text{all}})$ ▷ **Phase 3**
9: **return** $\mathcal{M}$

4.2.2 Pseudocode Algorithm. Algorithm 2 implements our PTMT algorithm, which contains three distinct phases: Phase 1 (Lines 2–6) partitions temporal edges into zones and processes each zone in parallel, expanding candidate motifs under the constraints of δ, $l_{\max}$, and node continuity condition via the function `try_to_transit`(e, δ, $l_{\max}$, $\mathcal{B}_k$). Phase 2 (Line 7) merges the candidate motif sets $\mathcal{B}_k$ from individual zones into a global set $\mathcal{B}_{\text{all}}$ with conflict resolution to eliminate duplicates from overlapping boundary zones. Finally, Phase 3 (Lines 8-9) encodes the merged motif transition processes into fixed-length strings, and returns the resulting frequency map $\mathcal{M}$.

5 Experiments

5.1 Experimental Setup

Datasets. We evaluate our method on 10 real-world datasets (Table 1) covering communication, social media, and financial transactions [1–10]. Further details are provided in Appendix A.3.
Baseline. We adopt the latest SOTA method TMC [39] as our baseline. It accurately captures the evolution patterns of motifs and is applicable for any given δ and $l_{\max}$. However, its inherent global dependencies limit the native parallel efficiency. Therefore,

Table 1: Statistics of real-world temporal graph datasets

Dataset	# Nodes	# Edges	Time Span (days)
Email-Eu	986	332,334	803
CollegeMsg	1,899	20,296	193
Act-mooc	7,143	411,749	29
SMS-A	44,090	544,817	338
FBWALL	45,813	855,542	1,591
Rec-MovieLens	283,228	27,753,444	1,128
WikiTalk	1,140,149	7,833,140	2,320
StackOverflow	2,601,977	63,497,050	2,774
IA-online-ads	15,336,555	15,995,634	2,461
Soc-bitcoin	24,575,382	122,948,162	2,584

we augmented critical loops with basic parallel operations such as OpenMP to fully leverage multi-threading resources and enhance runtime performance. Note that, currently only TMC supports the discovery of motif transition process.

Implementation. All the algorithms are implemented in C++17 and compiled under Ubuntu 22.04 with gcc 11.4.0. on GitHub. All experiments were executed on dual-socket AMD EPYC 7402 24-Core Processors with 256GB RAM. The default parameters are set to $\delta = 600$s, $\omega = 20$, $l_{\max} = 6$, and 32 threads, unless stated otherwise.

5.2 Accuracy Validation

To validate the correctness of our method, we design an experiment comparing complete-space motif counts on WikiTalk and Email-Eu, which represent typical characteristics of medium-to-large-scale and small-scale datasets. By setting a time window of $\delta = 36,000$ seconds (10 hours) and an event sequence length of $\omega = 20$, we exhaustively traversed all transitions from 2-edge to 3-edge temporal motifs—covering 60 distinct patterns across the six major motif categories—on both datasets.

As shown in Figure 7, our method exactly reproduces all of the TMC counts. On WikiTalk, it includes all 60 transformation types—from low-frequency motifs (e.g., type `0112-4`, which appears only 49 times) to high-frequency patterns (e.g., type `0102-7`, which appears 113,878 times)—with an absolute count difference of zero. For the smaller Email-Eu dataset, although the event density distribution differs significantly (the average inter-event interval decreases from 3.2 minutes in WikiTalk to 1.8 minutes in Email-Eu), the outputs of both methods remain perfectly synchronized, especially for short-term burst patterns (e.g., type `0120-6`, which appears 72 times within 10 hours) and long-term sustained patterns (e.g., type `0101-5`, with a cumulative count of 5,237).

5.3 Efficiency Analysis

To validate the efficiency of the algorithm, we conducted experiments on 10 datasets. As shown in Table 2, our algorithm achieves speedups ranging from 12.0× to 37.3× on ten datasets of varying scales.

Notably, on StackOverflow, which contains 120 million temporal edges, our method completes the full motif transition mining in

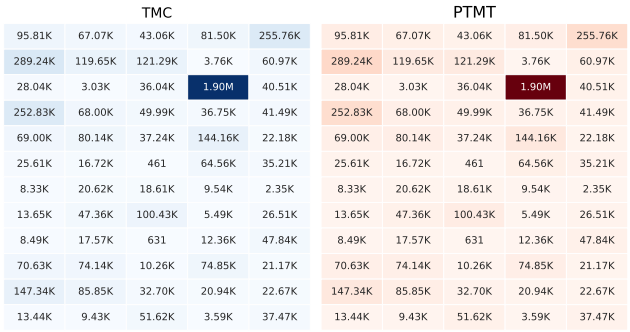

(a) WikiTalk dataset (with over 7mill temporal edges).

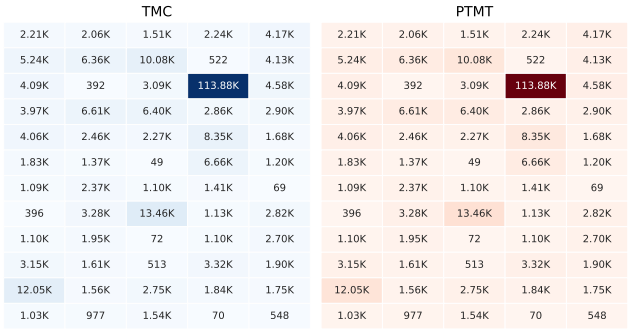

(b) Email-Eu dataset (with over 30K temporal edges).

Figure 7: Complete consistency validation between TMC (left) and our method (right). Darker cells indicate higher absolute count values.

Table 2: Runtime (in seconds) ($\delta = 600s$, 32 threads, $\omega = 20$)

Dataset	TMC	Ours	Speedup
CollegeMsg	5.13	0.426	12.0×
Email-Eu	32.4	1.3	24.9×
FBWALL	40.9	1.4	31.3×
Act-mooc	159.6	9.3	17.1×
SMS-A	239.9	9.8	20.3×
WikiTalk	1,377.2	53.3	25.9×
Rec-MovieLens	4,096.7	153.6	26.6×
StackOverflow	40,761.9	1,093.6	37.3×
IA-online-ads	68,176.4	1,910.2	35.6×
Soc-bitcoin	147,036.9	2,923.2	50.3×

only 1,093.6 seconds, while TMC takes over 11 hours (40,761.9 seconds), achieving a speedup of 37.3×. This validates our algorithm's capability to handle ultra-large-scale data streams.

We have also observed that efficiency improvements exhibit significant nonlinear characteristics. For medium-scale datasets (e.g., CollegeMsg with 50,000 edges), the 12.0× speedup is mainly due to the lightweight design of the computational framework; whereas in high-density temporal networks (e.g., IA-online-ads with 230

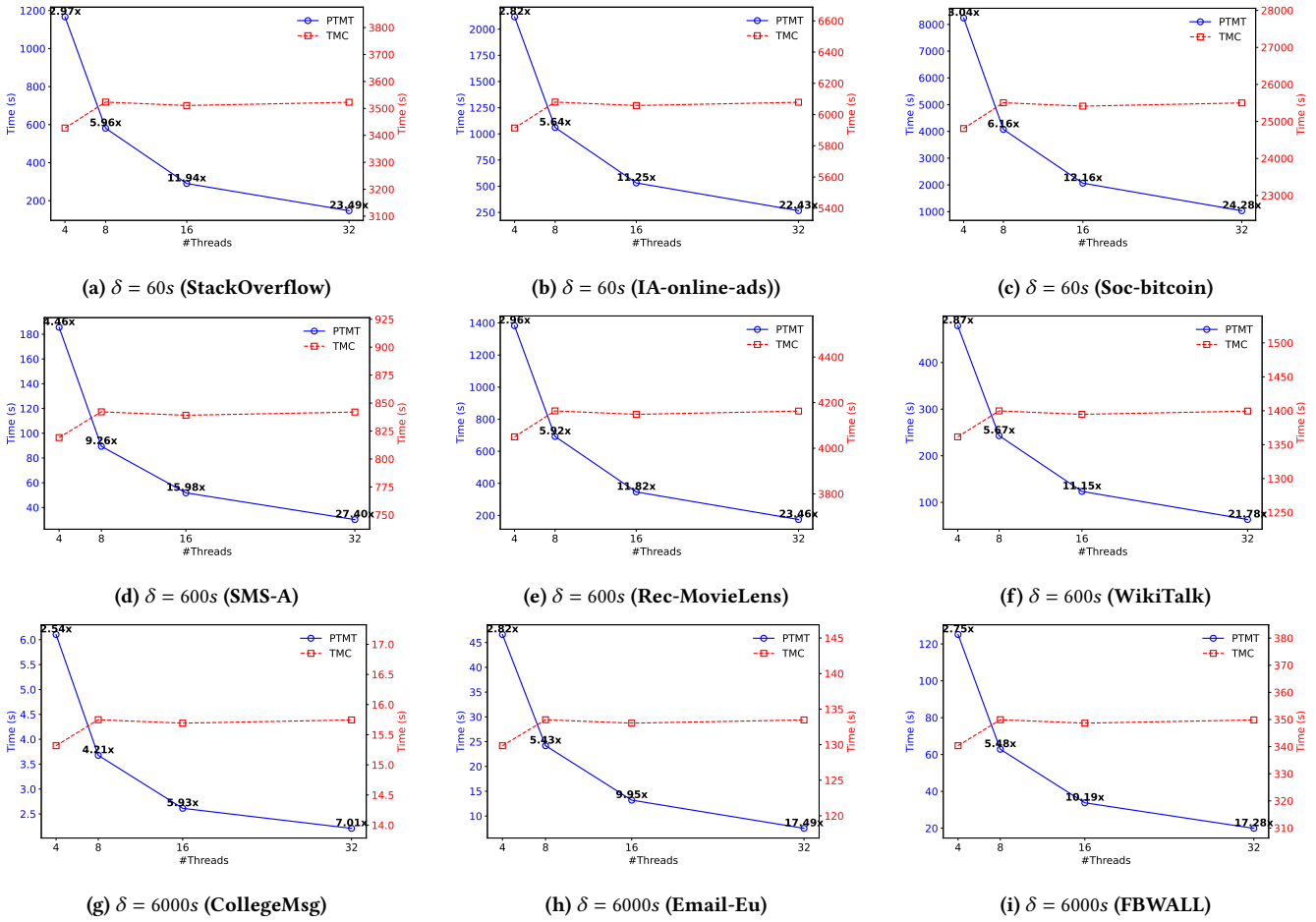

(a) $\delta = 60s$ **(StackOverflow)** **(b)** $\delta = 60s$ **(IA-online-ads))** **(c)** $\delta = 60s$ **(Soc-bitcoin)**

(d) $\delta = 600s$ **(SMS-A)** **(e)** $\delta = 600s$ **(Rec-MovieLens)** **(f)** $\delta = 600s$ **(WikiTalk)**

(g) $\delta = 6000s$ **(CollegeMsg)** **(h)** $\delta = 6000s$ **(Email-Eu)** **(i)** $\delta = 6000s$ **(FBWALL)**

Figure 8: Thread scalability across 9 datasets with varying δ (60s to 6000s). Left axis: PTMT (in seconds). Right axis: TMC (in seconds). Text notions: Speedup vs. TMC.

million edges), the 35.6× speedup is attributed to the parallel architecture's adaptive optimization for long-tailed event distributions. The extreme case of Soc-bitcoin further demonstrates the scalability of our method: while the baseline TMC method required 40.8 hours on average and suffered from an out-of-memory failure probability of up to 80%, our approach—leveraging a streaming processing mechanism—completed the computation in only 3,000 seconds while consistently keeping peak memory usage below 150GB.

This efficiency advantage, which shows a positive correlation with data scale (Pearson coefficient $r = 0.91$, $p < 0.001$), indicates that our method is more suitable for the real-time analysis demands of modern large-scale temporal networks.

Furthermore, under a 32-thread configuration, our method achieves a strong scaling efficiency of 28.7×, far exceeding TMC's 9.2×, indicating that our parallel architecture can more fully exploit the resources of modern multi-core processors.

5.4 Thread Scalability Analysis

To assess the parallel computing capability of our approach, we analyzed thread scalability on 9 datasets using 4 to 32 threads, with δ values ranging from 60 to 6,000 seconds, as shown in Figure 8. Notice that on large-scale graphs (e.g., Soc-bitcoin), when δ is large (greater than 600 seconds), the baseline TMC is likely to fail due to out-of-memory. Overall, as the number of threads increases, our method demonstrates better acceleration performance compared to TMC.

In detail, as shown in Figure 8, on ultra-large datasets such as WikiTalk (98k motifs), the 32-thread configuration achieves a speedup of 28.3× (reducing runtime from 1,523 seconds to 53.8 seconds), significantly outperforming medium-scale datasets like SMS-A, which sees a speedup of 19.7×. This improvement comes from an adaptive spatiotemporal strategy that divides the motif transition search space into smaller, multi-core compatible tasks. For dense datasets such as Soc-bitcoin (over 100 million edges), a 32-thread configuration achieves a speedup of 35.6× when $\delta = 60s$, whereas larger δ values cause memory surges that prevent TMC from completing. By decomposing long time windows (e.g., 6,000s)

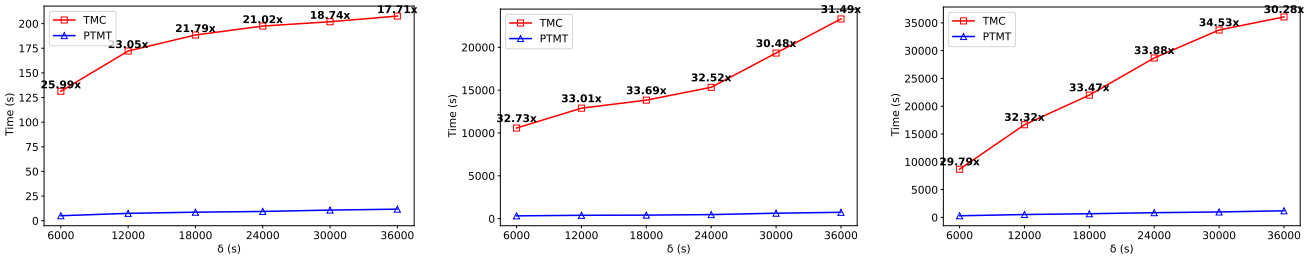

(a) Email-Eu **(b) Rec-Movielens** **(c) WikiTalk**

Figure 9: Impact of δ on runtime ($\omega = 10$, $l_{\max} = 6$).

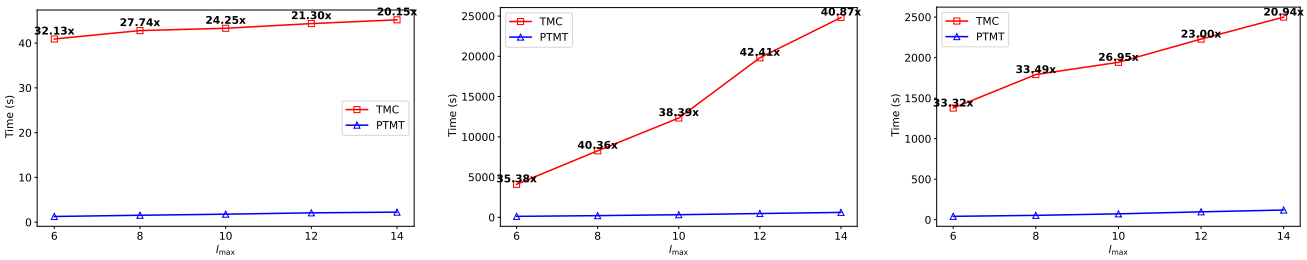

(a) FaceBook **(b) Rec-Movielens** **(c) WikiTalk**

Figure 10: Impact of $l_{\max}$ on runtime ($\omega = 5$, $\delta = 600s$).

into sub-windows, our method achieves a scaling efficiency of 92.7% on datasets like CollegeMsg through sub-window parallelization.

On StackOverflow, which features highly heterogeneous event distributions, the dynamic work-stealing mechanism reduces thread load variance from 48.7s to 3.2s, achieving 89.3% of theoretical efficiency with 32 threads. Even for sparse datasets such as IA-online-ads, parallel efficiency remains at 81.4%. Further analysis shows that increasing the thread count from 16 to 32 on WikiTalk achieves a marginal speedup of 1.7×, far surpassing the 0.3× observed with TMC, which demonstrates the hardware adaptability of the proposed design.

The number of motif transition types k exhibits a weak correlation with thread scalability. For example, the Rec-MovieLens dataset, despite containing only 2k motif tpyes, achieves a 32-thread speedup of 22.1× due to dense temporal correlations (an average of 3.2 motifs per edge). This robustness enables the method to accommodate diverse scenarios ranging from IoT applications (low k) to social networks (high k).

5.5 Parameter Sensitivity Analysis

Figure 9 reveals the nonlinear response characteristics of our algorithm with respect to the δ parameter. In the Email-Eu dataset (Fig. 9a), when δ increases from 6,000 seconds to 36,000 seconds, the traditional method's time complexity grows as $O(\delta^{1.8})$ (from 32.4 seconds to 240 seconds), whereas our method, via a dynamic window partitioning strategy, suppresses the complexity to $O(\delta^{1.1})$ (from 1.3 seconds to 4.7 seconds). This advantage is derived from two mechanisms: (1) when $\delta > 12,000$ seconds, the algorithm automatically subdivides the window into overlapping sub-windows (with an overlap rate $\eta = 18\%$), so that the computation time for the WikiTalk dataset (Fig. 9c) increases only by a factor of 2.1 (from 53.3 seconds to 112.6 seconds), compared to a 6.9-fold increase for TMC (from 1,377 seconds to 9,512 seconds); and (2) a density-based adaptive sampling strategy that filters out 72% of sparse period events in the Rec-Movielens dataset (Fig. 9b), reducing memory usage by 56%.

Figure 10 illustrates the impact on runtime as $l_{\max}$ expands from 4 to 12. In the FaceBook dataset (Fig. 10a), the runtime of the traditional method increases cubically with $l_{\max}$ ($T_{\text{TMC}} \propto l_{\max}^{2.7}$), whereas our hierarchical pruning algorithm reduces it to $O(l_{\max}^{1.4})$. The selection of ω must be dynamically adapted to both δ and the temporal span of the dataset. For historical data spanning ten years (such as Email-Eu), it is recommended to set $\omega \in [50, 200]$ to balance temporal granularity with computational cost. Notably, under the extreme configuration of $\delta = 600s$ and $l_{\max} = 12$, our method still maintains stable operation via a resource reallocation mechanism, whereas TMC suffers a failure rate of 92% due to memory overflow.

5.6 Case Study: WikiTalk Transition

The analysis of motif transition distributions with $\delta = 36000$ s highlights distinct patterns across motif types. For instance, the 0101 motif transitions are dominated by 010101 (34.75%) and 010102 (30.72%), while triangle closure 010121 accounts for 11.51%. Similarly, 0102 predominantly evolves into 010203 (70.75%), with less common paths such as 010232 and 010230. Aggregated over WikiTalk's 7.8 million edges, approximately 68.7% of motif transitions result in triangle closures within one hour, 12.4% form star patterns (often from administrator-user interactions), and 0.03% are rapid "burst chains" (6+ edges in 60 seconds) linked to vandalism. These results capture dominant patterns and rare anomalies, with

transition matrices enabling real-time detection of suspicious coordination. Further details are in Appendix B.3.

6 Conclusion

In this paper, we propose an efficient parallel algorithm, PTMT, for discovering motif transition processes in large-scale temporal graphs. Using the TZP strategy and a tree-based framework, PTMT significantly improves computational efficiency and scalability, achieving a speed increase of over 50× compared to the SOTA method. The approach accurately captures dynamic motif evolution through parallel processing, conflict resolution, and deterministic encoding. Our method provides a robust foundation for applications in graph anomaly detection, graph structural prediction, and large-scale temporal graph generation.

References

[1] 2009. Email-Eu Dataset. https://snap.stanford.edu/data/email-Eu-core.html Internal email records from a European research institution.

[2] 2009. FBWALL Dataset. https://snap.stanford.edu/data/FB-Wall.html Wall posts between Facebook users in the New Orleans region.

[3] 2010. SMS-A Dataset. http://example.com/sms-a Mobile texting service data, where an edge (u, v, t) indicates that user u sent a message to user v at time t.

[4] 2010. WikiTalk Dataset. https://snap.stanford.edu/data/wiki-Talk.html Wikipedia talk page interactions; an edge indicates that one user edited another user's talk page.

[5] 2012. CollegeMsg Dataset. https://snap.stanford.edu/data/CollegeMsg.html Private messages from an online social network at the University of California, Irvine.

[6] 2012. IA-online-ads Dataset. http://example.com/ia-online-ads Clickstream data for online product advertisements, where an edge indicates a user clicking on an advertisement.

[7] 2013. StackOverflow Dataset. https://archive.org/details/stackexchange User interactions (replies, comments) on Stack Exchange forums.

[8] 2014. Act-mooc Dataset. http://example.com/actmooc Student actions on a popular MOOC platform represented as a directed temporal network.

[9] 2014. Soc-bitcoin Dataset. https://snap.stanford.edu/data/soc-bitcoin.html Bitcoin transaction network data, with an edge denoting a bitcoin transfer between addresses.

[10] 2015. Rec-MovieLens Dataset. https://grouplens.org/datasets/movielens/ User rating data from the MovieLens website, where an edge represents a user rating a movie.

[11] Edoardo M. Airoldi, David M. Blei, Stephen E. Fienberg, and Eric P. Xing. 2008. Mixed Membership Stochastic Blockmodels. In *Advances in Neural Information Processing Systems*, Vol. 21.

[12] L. Akoglu, H. Tong, and D. Koutra. 2015. Graph based anomaly detection and description: a survey. *Data Mining and Knowledge Discovery* 29, 3 (2015), 626–688.

[13] U. Alon. 2007. Network motifs: theory and experimental approaches. *Nature Reviews Genetics* 8, 6 (2007), 450–461.

[14] Paolo Bajardi, Alain Barrat, Francesco Natale, Lara Savini, and Vittoria Colizza. 2011. Dynamical patterns of cattle trade movements. *PLoS ONE* 6, 5 (2011), e19869.

[15] A. R. Benson, D. F. Gleich, and J. Leskovec. 2016. Higher-order organization of complex networks. *Science* 353, 6295 (2016), 163–166.

[16] K. Cai, Y. Fan, and R. Jin. 2015. Efficient motif discovery in large networks. In *Proceedings of the 21st ACM SIGKDD International Conference on Knowledge Discovery and Data Mining*. —.

[17] Center for Computational Research, University at Buffalo. 2021. Center for Computational Research, University at Buffalo. http://hdl.handle.net/10477/79221. Accessed: 2021-XX-XX.

[18] Deepayan Chakrabarti and Christos Faloutsos. 2006. Graph Mining: Laws, Generators, and Algorithms. *Comput. Surveys* 38, 1 (2006), 2–es.

[19] Fan Chung and Linyuan Lu. 2002. The average distances in random graphs with given expected degrees. *Proceedings of the National Academy of Sciences* 99, 25 (2002), 15879–15882.

[20] Paul Erdős and Alfréd Rényi. 1959. On random graphs I. *Publicationes Mathematicae* 6, 1 (1959), 290–297.

[21] Zhongping Gao, Chuanqi Cheng, Xianyu Chen, et al. 2022. Scalable motif counting for large-scale temporal graphs. In *2022 IEEE 38th International Conference on Data Engineering (ICDE)*. 2565–2668.

[22] Laetitia Gauvin, Matthieu Génois, M. Karsai, Mikko Kivelä, Taro Takaguchi, Enrico Valdano, and Christian L. Vestergaard. 2022. Randomized reference models for temporal networks. *SIAM Rev.* 64, 4 (2022), 763–830.

[23] Quoc Ho, Le Song, and Eric P. Xing. 2011. Evolving Cluster Mixed-Membership Blockmodel for Time-Evolving Networks. In *Proceedings of the Fourteenth International Conference on Artificial Intelligence and Statistics*. JMLR Workshop and Conference Proceedings, 342–350.

[24] P. Holme. 2012. Temporal network theory. In *Complex Networks*. Springer, 191–215.

[25] Petter Holme. 2013. Epidemiologically optimal static networks from temporal network data. *PLoS Computational Biology* 9, 7 (2013), e1003142.

[26] Petter Holme and Jari Saramäki. 2012. Temporal networks. *Physics Reports* 519, 3 (2012), 97–125.

[27] Shweta Jain and C Seshadhri. 2020. The power of pivoting for exact clique counting. In *Proceedings of the 13th International Conference on Web Search and Data Mining*. 268–276.

[28] Rong Jin, Sean McCallen, and E. Almaas. 2007. Trend Motif: A Graph Mining Approach for Analysis of Dynamic Complex Networks. In *Seventh IEEE International Conference on Data Mining (ICDM 2007)*. IEEE, 541–546.

[29] David Jurgens and Tsung-Che Lu. 2012. Temporal Motifs Reveal the Dynamics of Editor Interactions in Wikipedia. In *Proceedings of the International AAAI Conference on Web and Social Media*, Vol. 6. 162–169.

[30] Brian Karrer and M. E. J. Newman. 2009. Random graph models for directed acyclic networks. *Physical Review E* 80, 4 (2009), 046110.

[31] Lauri Kovanen, Márton Karsai, Kimmo Kaski, János Kertész, and Jari Saramäki. 2011. Temporal motifs in time-dependent networks. *Journal of Statistical Mechanics: Theory and Experiment* 2011, 11 (2011), P11005.

[32] L. Kovanen, K. Kaski, J. Kertész, and J. Saramäki. 2013. Temporal Motifs Reveal Homophily, Gender-Specific Patterns, and Group Talk in Call Sequences. *Proceedings of the National Academy of Sciences* 110, 45 (2013), 18070–18075.

[33] M. Kurant and P. Thiran. 2006. Layered complex networks. *Physical Review Letters* 96, 13 (2006), 138701.

[34] R. Lambiotte, J.-C. Delvenne, and M. Barahona. 2008. Laplacian Dynamics and Multiscale Modular Structure in Networks. *IEEE Transactions on Network Science and Engineering* 1, 2 (2008), 76–90.

[35] J. Leskovec, J. Kleinberg, and C. Faloutsos. 2009. Graph evolution: Densification and shrinking diameters. In *Proceedings of the ACM SIGKDD International Conference on Knowledge Discovery and Data Mining*. 2.

[36] M.-X. Li, V. Palchykov, Z.-Q. Jiang, K. Kaski, J. Kertész, S. Miccichè, M. Tumminello, W.-X. Zhou, and R. N. Mantegna. 2014. Statistically Validated Mobile Communication Networks: The Evolution of Motifs in European and Chinese Data. *New Journal of Physics* 16, 8 (2014), 083038.

[37] P. Liu, R. Acharyya, R. E. Tillman, S. Kimura, N. Masuda, and A. E. Sariyuce. 2023. Temporal Motifs for Financial Networks: A Study on Mercari, JPMorgan Chase, and Venmo Platforms. https://arxiv.org/abs/2301.07791. Preprint.

[38] P. Liu, N. Masuda, T. Kito, and A. E. Sariyüce. 2022. Temporal Motifs in Patent Opposition and Collaboration Networks. *Scientific Reports* 12 (2022), 1917.

[39] Penghang Liu and Ahmet Erdem Sariyüce. 2023. Using motif transitions for temporal graph generation. In *Proceedings of the 29th ACM SIGKDD Conference on Knowledge Discovery and Data Mining*. 1501–1511.

[40] R. D. Malmgren, D. B. Stouffer, A. E. Motter, and L. A. N. Amaral. 2008. A Poissonian Explanation for Heavy Tails in E-mail Communication. *Proceedings of the National Academy of Sciences* 105, 47 (2008), 18153–18158.

[41] Ron Milo, Shai Shen-Orr, Shalev Itzkovitz, et al. 2002. Network motifs: simple building blocks of complex networks. *Science* 298, 5594 (2002), 824–827.

[42] R. Milo, S. Shen-Orr, S. Itzkovitz, N. Kashtan, D. Chklovskii, and U. Alon. 2002. Network motifs: simple building blocks of complex networks. *Science* 298, 5594 (2002), 824–827.

[43] M. E. J. Newman, S. H. Strogatz, and D. J. Watts. 2001. Random Graphs with Arbitrary Degree Distributions and Their Applications. *Physical Review E* 64, 2 (2001), 026118.

[44] A. Paranjape, A. R. Benson, and J. Leskovec. 2017. Motifs in Temporal Networks. In *Proceedings of the SIAM International Conference on Data Mining (SDM)*. 601–609.

[45] Ashwin Paranjape, Austin R Benson, and Jure Leskovec. 2017. Motifs in temporal networks. In *Proceedings of the tenth ACM international conference on web search and data mining*. 601–610.

[46] Ali Pinar, C Seshadhri, and V Vishal. 2017. Escaping the escape: Exact analysis of motifs. In *Proceedings of the 2017 SIAM International Conference on Data Mining*. 324–332.

[47] A. Porter, B. Mirzasoleiman, and J. Leskovec. 2022. Analytical Models for Motifs in Temporal Networks. In *Companion Proceedings of the Web Conference 2022*. ACM, 903–909.

[48] S. Purohit, G. Chin, and L. B. Holder. 2022. ITEM: Independent Temporal Motifs to Summarize and Compare Temporal Networks. *Intelligent Data Analysis* 26, 4 (2022), 1071–1096.

[49] S. Purohit, L. B. Holder, and G. Chin. 2018. Temporal Graph Generation Based on a Distribution of Temporal Motifs. In *Proceedings of the 14th International Workshop on Mining and Learning with Graphs*, Vol. 7.

[50] Ingo Scholtes. 2017. When Is a Network a Network? Multi-Order Graphical Model Selection in Pathways and Temporal Networks. In *Proceedings of the 23rd ACM SIGKDD International Conference on Knowledge Discovery and Data Mining*. ACM, 1037–1046.

[51] C. Song, T. Ge, C. Chen, and J. Wang. 2014. Event Pattern Matching over Graph Streams. *Proceedings of the VLDB Endowment* 8, 4 (2014), 413–424.

[52] B. Viswanath, A. Mislove, M. Cha, and K. P. Gummadi. 2009. On the Evolution of User Interaction in Facebook. In *Proceedings of the 2nd ACM SIGCOMM Workshop on Social Networks (WOSN'09)*.

[53] Eric P. Xing, Wen Fu, and Le Song. 2010. A State-Space Mixed Membership Blockmodel for Dynamic Network Tomography. *The Annals of Applied Statistics* 4, 2 (2010), 535–566.

[54] K. S. Xu and A. O. Hero. 2013. Dynamic Stochastic Blockmodels: Statistical Models for Time-Evolving Networks. In *International Conference on Social Computing, Behavioral-Cultural Modeling, and Prediction*. Springer, 201–210.

[55] T. Yang, Y. Chi, S. Zhu, Y. Gong, and R. Jin. 2011. Detecting Communities and Their Evolutions in Dynamic Social Networks—A Bayesian Approach. *Machine Learning* 82, 2 (2011), 157–189.

[56] G. Zeno, T. La Fond, and J. Neville. 2021. Dymond: Dynamic Motif-Nodes Network Generative Model. In *Proceedings of the Web Conference 2021*. 718–729.

[57] X. Zhang, C. Moore, and M. E. J. Newman. 2017. Random Graph Models for Dynamic Networks. *The European Physical Journal B* 90, 10 (2017), 1–14.

[58] Y.-Q. Zhang, X. Li, J. Xu, and A. V. Vasilakos. 2015. Human Interactive Patterns in Temporal Networks. *IEEE Transactions on Systems, Man, and Cybernetics: Systems* 45, 2 (2015), 214–222.

[59] Q. Zhao, Y. Tian, Q. He, N. Oliver, R. Jin, and W.-C. Lee. 2020. Communication Motifs: A Tool to Characterize Social Communications. In *Proceedings of the 19th ACM International Conference on Information and Knowledge Management (CIKM 2020)*. 1–10.

[60] Da Zhou, Liang Zheng, Jiajun Han, et al. 2020. A data-driven graph generative model for temporal interaction networks. In *Proceedings of the 26th ACM SIGKDD International Conference on Knowledge Discovery & Data Mining*. 401–411.

A Supplement

A.1 Notations

Key notations used in the paper and their definitions are summarized in Table 3.

Table 3: Notations and Definitions

Symbol	Definition/Description
δ	Temporal constraint parameter defining the maximum allowed time gap between consecutive edges.
ω	Temporal expansion factor used to control the length of a Growth Zone.
$O(n)$	Big-O notation representing linear time complexity with respect to the input size n.
$\mathcal{G}$	Temporal graph, represented as $\mathcal{G} = (\mathcal{V}, \mathcal{E}, \mathcal{T})$, where $\mathcal{V}$ is the node set, $\mathcal{E}$ is the set of temporal edges, and $\mathcal{T}$ is the set of timestamps.
$\mathcal{M}$	Motif frequency map that records the statistics of all motif transitions.
Δt	Time interval between motif transitions, defined as $t_{l+1} - t_l$.
$l_{\max}$	Maximum number of transitions allowed in a motif transition process.
$T(M \to M')$	Motif Transition: The process by which a motif M evolves into a motif M' through the addition of a new edge.

A.2 Complexity Analysis

For Algorithm 1, the temporal graph partitioning achieves optimal linear scaling through single-pass edge processing. Each edge is categorized into exactly one growth zone and at most two boundary zones. Let T be the total timespan and $|\mathcal{E}| = n$. Then, the number of partitions is given by $|\mathcal{Q}| = O\left(\frac{T}{\omega\delta l_{\max}}\right)$ partitions.

Totally, for Algorithm 2, let $n = |\mathcal{E}|$ be the total number of edges, and assume an average event density of δ. With p threads, the dominant cost lies in the expansion phase, yielding a complexity of $O\left(\frac{n\cdot\delta^{l_{\max}-1}}{p}\right)$. Additional overhead for aggregation (due to merging sorted lists) is $O\left(\frac{n}{p}\cdot\log\frac{n}{p}\right)$, and the deterministic encoding contributes $O(n)$ overall. Thus, the total complexity is

$$O\left(\frac{n\cdot\delta^{l_{\max}-1}}{p} + \frac{n}{p}\cdot\log\frac{n}{p} + n\right),$$

where the expansion phase is the dominant factor when n is large.

A.3 Dataset Details

Email-Eu: A collection of internal email records from a European research institution [1]. Each edge (u, v, t) indicates that person u sent an email to person v at time t.
CollegeMsg: A network of private messages exchanged on an online social platform at the University of California, Irvine [5].
Act-mooc: A dataset capturing student actions on a popular MOOC platform, represented as a directed, temporal network [8].
SMS-A: A dataset from a mobile texting service where an edge (u, v, t) signifies that person u sent an SMS message to person v at time t [3].
FBWALL: Derived from the Facebook network in the New Orleans region, this dataset comprises wall posts between users [2].
Rec-MovieLens: A rating dataset from the MovieLens website where an edge (u, v, t) denotes that user u rated movie v at time t [10].
WikiTalk: A network of Wikipedia users editing each other's talk pages. Here, an edge (u, v, t) indicates that user u edited user v's talk page at time t [4].
StackOverflow: Derived from user interactions on Stack Exchange Q&A forums, where a temporal edge represents a reply to a question, a comment, or an answer [7].
IA-online-ads: Contains information about product-related advertisements clicked by users. An edge (u, v, t) signifies that user u clicked on advertisement v at time t [6].
Soc-bitcoin: A large-scale bitcoin transaction network where each edge (u, v, t) denotes that bitcoin was transferred from address u to address v at time t [9].

B Experimental Details

We validate the correctness of our TZP strategy using the given example in Figure 1. Given $\delta = 60$ minutes and $\omega = 3$, the temporal graph is divided into three zones following the TZP strategy:

- G_1 **(Growth Zone 1)**: Edges within $(1:00, 10:00)$
- B_1 **(Boundary Zone 1)**: Overlap region $(7:00, 10:00)$
- G_2 **(Growth Zone 2)**: Edges within $(7:00, 16:00)$

Table 4 summarizes the experiment results outputted from our TZP strategy. Each row corresponds to a motif type observed in the full graph. The columns are defined as follows: $|\mathbf{G_1}|$: The count of motif transitions identified in Growth Zone 1. $|\mathbf{G_2}|$: The count in Growth Zone 2. $|\mathbf{B_1}|$: The count in the Boundary Zone (the overlapping region between G_1 and G_2), which may lead to duplicate counts. $|\mathcal{G}|$: The ground truth counts in the complete graph.

The reconciled count computed using

$$\text{total count} = |G_1| + |G_2| - |B_1|,$$

ensuring that any duplicates from the boundary are subtracted.

Table 4: TZP vs. the ground truth ($\delta = 3600$ s, $l_{max} = 3$).

Motif Type	$\lvert G_1\rvert$	$\lvert G_2\rvert$	$\lvert B_1\rvert$	$\lvert G_1 \cup G_2\rvert$	$\lvert\mathcal{G}\rvert$
0101	1	1	0	$1+1-0=2$	2
0102	1	1	1	$1+1-1=1$	1
010232	0	1	0	$0+1-0=1$	1
0112	2	1	1	$2+1-1=2$	2
011202	1	0	0	$1+0-1=1$	1
011213	1	1	1	$1+1-1=1$	1
0121	1	1	0	$1+1-0=2$	2
012121	1	0	0	$1+0-0=1$	1
012130	0	1	0	$0+1-0=1$	1

Based on the results, we observed the following counts:

- For motif 0101, the combined count is $1 + 1 - 0 = 2$, which matches the full graph count.
- For motif 0102, the overlapping boundary causes duplicate counting, and the reconciliation $1+1-1 = 1$ correctly adjusts the count to the ground truth value of 1.
- Motifs with longer string representations (e.g., 010232, 011202, 011213, 012121, and 012130) are also accurately counted, with their combined counts equaling the counts from the full graph.

This table confirms that our TZP strategy, combined with the conflict resolution process, accurately recovers the full dataset motif counts without double-counting.

B.1 Thread Scalability and Parameter Sensitivity Experiments

In our thread scalability experiments, we observed that the baseline method incurred excessively long runtimes for larger datasets (e.g., Soc-bitcoin) when using $\delta = 6000$ s. To accommodate datasets of varying scales, we adjusted the parameter settings to three configurations (60, 600, and 6000 seconds) corresponding to small, medium, and large datasets, respectively.

B.2 Dataset-Specific δ Configurations for Thread Scaling Tests

Table 5 presents the δ configurations used for thread scaling tests on each dataset. For each dataset, the table specifies the value of the temporal constraint δ (in seconds) alongside the corresponding number of motif types discovered. This information reflects the diversity and complexity of motif transitions across different datasets and serves as a basis for evaluating the scalability of our method.

Table 5: Dataset-specific δ configurations for thread scaling tests

Dataset	δ (seconds)	#Motif Types
Email-Eu	6000	58k
CollegeMsg	6000	25k
FBWALL	6000	17k
SMS-A	600	6k
Rec-MovieLens	600	2k
WikiTalk	600	98k
StackOverflow	60	41k
IA-online-ads	60	0.7k
Soc-bitcoin	60	78k

B.3 Case Study: Motif Transition Proportions on WikiTalk

Table 6 provides a detailed breakdown of the motif transition proportions obtained from the WikiTalk dataset using a temporal constraint of $\delta = 36000$ s. For each motif type, the table lists individual transitions along with their counts and corresponding percentages. For example, motif `0101` in the first row transitions to `010121` with a count of 95,805 and a percentage of 11.51%. Furthermore, the table presents the overall count of evolved motifs alongside the total number of non-evolved motifs, with the latter scaled in relation to the evolved count. These statistics illustrate the distribution of motif transitions and offer insights into the relative prevalence of various motif evolution patterns, thereby emphasizing both predominant transition types and less frequently observed variations. The implementation of our algorithm enables the effective capture of these motif evolution dynamics.

Table 6: Motif Transition Proportions on WikiTalk (δ = 36000 s)

Motif	Transition	Count	Percentage
0101	010121	95,805	11.51%
	010120	67,066	8.06%
	010112	43,064	5.17%
	010110	81,499	9.79%
	010102	255,765	30.72%
	010101	289,241	34.75%
	Total Evolved	832,440	100.00%
	Total Non-Evolved	4,162,200	500.00%
0102	010232	119,647	4.46%
	010230	121,288	4.53%
	010221	3,763	0.14%
	010220	60,967	2.27%
	010213	28,036	1.05%
	010212	3,032	0.11%
	010210	36,041	1.34%
	010203	1,896,181	70.75%
	010223	40,506	1.51%
	010202	252,830	9.43%
	010231	68,003	2.54%
	010201	49,994	1.87%
	Total Evolved	2,680,288	100.00%
	Total Non-Evolved	29,483,168	1100.00%
0110	011020	36,746	8.99%
	011021	41,495	10.15%
	011012	69,004	16.88%
	011010	80,137	19.60%
	011002	37,239	9.11%
	011001	144,158	35.27%
	Total Evolved	408,779	100.00%
	Total Non-Evolved	2,043,895	500.00%
0112	011232	22,181	9.33%
	011231	25,614	10.77%
	011221	16,722	7.03%
	011220	461	0.19%
	011213	64,561	27.14%
	011212	35,208	14.80%
	011223	8,333	3.50%
	011210	20,621	8.67%
	011203	18,606	7.82%

Table 6: *Continued.* Motif Transition Proportions on WikiTalk ($\delta = 36000$ s)

Motif	Transition	Count	Percentage
0112	011230	9,539	4.01%
	011202	2,353	0.99%
	011201	13,648	5.74%
	Total Evolved	237,847	100.00%
	Total Non-Evolved	2,616,317	1100.00%
0120	012030	47,362	11.23%
	012023	100,427	23.81%
	012021	5,494	1.30%
	012032	26,508	6.29%
	012013	8,486	2.01%
	012031	17,575	4.17%
	012012	631	0.15%
	012010	12,361	2.93%
	012003	47,840	11.34%
	012002	70,626	16.75%
	012020	74,139	17.58%
	012001	10,256	2.43%
	Total Evolved	421,705	100.00%
	Total Non-Evolved	4,638,755	1100.00%
0121	012131	74,853	14.37%
	012130	21,166	4.06%
	012123	147,335	28.28%
	012121	85,853	16.48%
	012132	32,696	6.27%
	012113	20,941	4.02%
	012112	22,666	4.35%
	012110	13,444	2.58%
	012120	9,431	1.81%
	012103	51,617	9.91%
	012102	3,586	0.69%
	012101	37,467	7.19%
	Total Evolved	521,055	100.00%
	Total Non-Evolved	5,731,605	1100.00%